Journal of
Materials Chemistry C

Accepted Manuscript

This article can be cited before page numbers have been issued, to do this please use: W. Fang, Z. Wang, P. Pei, R. Liu, Y. Zhang, L. Kong and J. Yang, *J. Mater. Chem. C*, 2018, DOI: 10.1039/C8TC02973C.

ROYAL SOCIETY OF CHEMISTRY

rsc.li/materials-c

View Article Online
DOI: 10.1039/C8TC02973C

Journal of Materials Chemistry C RSCPublishing

ARTICLE

Cite this: DOI: 10.1039/x0xx00000x

Received 00th January 2012,
Accepted 00th January 2012

DOI: 10.1039/x0xx00000x

www.rsc.org/

A Λ-shaped cyanostilbene derivative: multi-stimuli responsive fluorescence sensors, rewritable information storage and colour converter for w-LED

Wenyan Fang[a,b], Wang Zhao[b], Pan Pei[b], Rui Liu[b], Yuyang Zhang[a], Lin Kong[a], Jiaxiang Yang[a,c]*

A new Λ-shaped α-cyanostilbene derivative (**TSA**) containing active amino-group with fluorescence emission both in solution and solid state was designed, synthesized and characterized. Its colour and fluorescence emission can be switched by external stimuli including acid/base, trinitrophenol (picric acid, PA) and grinding. The ^{1}H NMR spectra of **TSA** were measured before and after alternately adding trifluoroacetic acid (TFA) and triethylamine (TEA), which confirmed that the acidichromism originated in the transformation of protonation/deprotonation between **TSA** and **TSA-H$^+$**. Powder X-ray diffraction (PXRD), differential scanning calorimetry (DSC) and scanning electron microscopy (SEM) revealed the crystalline-amorphous state transformation between the original and ground compounds, and this transformation could reasonably account for the mechanochromic (MFC) luminescent properties. The results revealed that **TSA** can be used as fluorescence sensors for acid/base and PA, and as rewritable information storage material. Moreover, it can also be applied in white light-emitting diode (w-LED) based on its desirable fluorescence emission in solid state.

1. Introduction

Stimuli-responsive organic fluorescent materials have attracted considerable interest due to their potential applications, such as fluorescent sensors,[1-2] bioimaging,[3-5] memory chips,[6-7] logic operation,[8-10] optical encoding,[11-12] optical switch,[13-14] data storage,[15-21] security paper or security ink,[21-27] and so on. Generally, most organic fluorescent materials suffer from an aggregation-caused quenching (ACQ) effect in the aggregate or solid state, which restricted the scope of their practical applications. On the contrary, aggregation-induced emission (AIE) or aggregation-induced enhanced emission (AIEE) contributes to the strong fluorescent emission in the solid-state but weak or even no emission in solution. Although some fluorescent materials could emit efficiently both in solution and solid state, they is only achieving in one system for multi-stimuli responsive applications. Therefore, developing multi-stimuli responsive fluorescent materials both in solution and in solid state for their applications in dual system remains a great challenge.

Recently, it is worth highlighting the significant interest in the α-cyanostilbene derivatives, because they have exhibited remarkable optical features and interesting electrical properties, and can be used to suitable and versatile option for the development of functional materials.[28] It is well known that a great number of α-cyanostilbene derivatives have the advantages of relatively simple synthetic procedures and AIE/AIEE-activity due to the steric and electronic effect of cyano group.[29-33] Although many stimuli-responsive properties of α-cyanostilbene derivatives have been reported, multi-stimuli responsive of them have been relatively less reported so far.

Currently, white light-emitting diodes (w-LEDs) have been investigated widely due to their extraordinary advantages, such as energy saving, environmental friendliness, high luminous efficiency, compact size, fast response time (10-20 ns) and long lifetime.[34-40] However, many commercial phosphor-converted w-LEDs employing inorganic phosphors still suffer some weaknesses, such as utilizing expensive rare-earth starting materials, the rigorous synthetic procedures (typically prepared under 1800 °C, 0.5 MPa N_2 pressure) and serious photon reabsorption phenomenon, and so on.[41-46] Hence, it is essential to synthesize organic small molecules luminescence materials applied in w-LEDs by using low-cost raw materials with simple and easily controlled synthesis procedures.

Based on the above considerations, in this work, a novel Λ-shaped α-cyanostilbene derivative (**TSA**) containing active

View Article Online
DOI: 10.1039/C8TC02973C

amino-group was designed and synthesized by introducing the α-cyanostilbene unit and active amino-group into structure of molecule. It is well known that the lone-pair electrons on N atoms which tend to accept protons and make it easier responsive for acid.[47-48] The synthesis process of the **TSA** is relatively simple. The **TSA** was characterized by FT-IR, ^{1}H NMR, ^{13}C NMR and mass spectroscopy, respectively. The luminescence properties and multi-stimuli responsive fluorescent for acid/base, PA and grinding of the **TSA** were studied. The results demonstrated that the **TSA** had fluorescence emission both in solution and solid state. The color and fluorescence emission of the **TSA** can be tuned by external stimuli including acid/base, PA and grinding. The results display that it can be used as indicator for acid/base and PA sensor and as information data storage material. Moreover, it can also be applied in white light-emitting diode (w-LED) on the basis of its desirable fluorescence emission in solid state.

2. Experimental

2.1. Materials and measurements

All chemicals with analytical grade were commercially available and were used without further purification. FT-IR spectra were obtained in KBr discs on a Nicolet 380 FT-IR spectrometer in the 4000-400 cm^{-1} region. ^{1}H and ^{13}C NMR spectra were recorded on a 400 MHz Bruker Avance spectrometer by using $CDCl_3$ or CD_3CN as solvent and tetramethylsilane (TMS) as an internal standard. Mass spectrum was obtained using an LC-MS (LTQ Orbitrap XL/LTQ Orbitrap XL). Thermogravimetric analysis (TGA) was performed on a Perkin Elmer Pyris 1 TGA Thermogravimetric Analyzer. Differential scanning calorimetry (DSC) curves were performed on DSC Q2000 in the temperature range from 25 to 300 °C at a heating rate of 10 °C min^{-1} under N_2 atmosphere. UV-vis absorption spectra of samples were recorded on an Ultraviolet, Visible, Near-Infrared spectrophotometer (U-4100). The fluorescence spectra of samples were measured with F-4500 fluorescence spectrophotometer. The absolute photoluminescence quantum yields (ΦF) of **TSA** in THF solution (1×10^{-5} M) and the solid state were determined using a Fluoromax-4 spectrophotometer with an integrating sphere. Powder X-ray diffraction (PXRD) patterns were measured using a Smart Lab X-ray diffractometer with Cu Kα radiation (λ = 1.54050 Å), operating in the 2θ range from 10° to 80°.The field emission scanning electron microscopy (FE-SEM) images were observed on a Jeol JSM-4800 scanning electronmicroscopy. Fluorescence lifetime test was carried out using an HORIBA FluoroMax-4P fluorescence spectrometer equipped with a time-correlated single-photon counting (TCSPC) card. The photoelectric parameters of the fabricated w-LED were measured using an Everfine HAAS-2000 spectroradiometer equipped with a barium sulfate coated integrating sphere and a CCD detector.

2.2. Synthesis of the target molecule

The synthesis route is shown in **Scheme 1**.

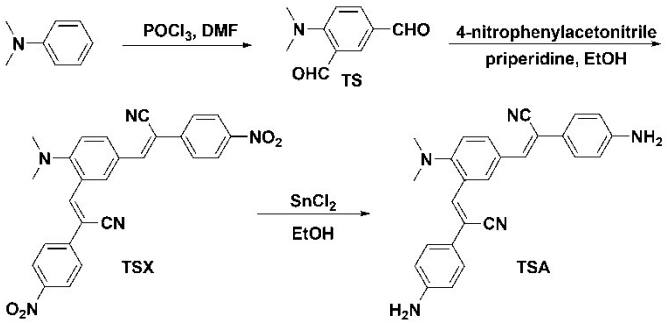

Scheme 1. Synthetic route of **TSA**.

2.2.1. Synthesis of compound TS

The $POCl_3$ (93.2 mL, 1 mol) was added by dropwise to dry DMF (77.4 mL, 1 mol), the mixture was stirred at ice-salt-bath until solidified. Then N,N-dimethylaniline (12.6 mL, 0.1 mol) was added to the mixture. The resultant mixture system was heated at 60 °C until they reacted completely monitoring by TLC. Subsequently the mixture was poured into ice water (300 mL) under stirring, and was neutralized with NaOH solution. Finally the mixture was extracted by dichloromethane (DCM). The combined organic layers were dried with $MgSO_4$ and the solvent was removed under vacuum. The crude product was purified by column chromatograph of silica gel with petroleum ether/ethyl acetate mixture (3/1, v/v) as the eluent to give **1** (13.51 g, off-whit filamentous solid) with the 76% yield. FT-IR (KBr, cm^{-1}): 2830 (w), 2746 (w), 2739 (w), 1662 (s), 1608 (s), 1527 (m), 1394 (m), 1259 (m), 1206 (m), 1180 (m), 1116 (m), 962 (m), 817 (m), 709 (m). ^{1}H NMR ($CDCl_3$, 400 MHz) δ: 10.04 (s, 1H), 9.85 (s, 1H), 8.19 (d, J = 2.1 Hz, 1H), 7.92 (dd, J_1 = 8.8 Hz, J_2 = 2.1 Hz, 1H), 7.02 (d, J = 8.8 Hz, 1H), 3.12 (s, 6H).

2.2.2 Synthesis and characterization of compound TSX

4-Nitrophenylacetonitrile (4.05 g, 0.025 mmol) was added to a solution of compound **TS** (1.77 g, 0.01 mol) in 100 mL of absolute ethanol. Then two drops of piperidine were added and the mixture was refluxed under stirring for a night. After cooling to room temperature, the precipitate was filtered and washed with ethanol for several times, then dried under vacuum giving rose red solid **TSX** 4.09 g (with a yield of 88%). FT-IR (KBr, cm^{-1}): 3076 (w), 2923 (w), 2210 (s), 1600 (w), 1565 (vs), 1511 (vs), 1430 (s), 1336 (vs), 1209 (s), 1108 (s), 854 (vs). ^{1}H NMR ($CDCl_3$, 400 MHz) δ: 8.34 (d, 2H, J = 8.8 Hz), 8.30 (m, 4H), 7.90 (d, 2H, J = 8.8 Hz), 7.85 (m, 3H), 7.65 (s, 1H), 7.18 (d, 1H, J = 8.4 Hz), 2.96 (s, 6H).

2.2.3. Synthesis and characterization of compound TSA

View Article Online
DOI: 10.1039/C8TC02973C

A mixture of (3.72 g, 8 mmol) **TSX** and $SnCl_2 \cdot H_2O$ (18.05 g, 80 mmol) in 100 mL of ethanol was heated to reflux monitoring by TLC. After the reaction finished and the mixture cooled to room temperature, the mixture pH was tuned to 8-9 with the saturated K_2CO_3 solution adding slowly under stirring. The resultant solution was extracted with ethyl acetate. The organic phase was dried with anhydrous Na_2SO_4 and concentrated in vacuum. The crude product was purified by column chromatography using DCM eluent and then recrystallized with ethanol to give the pale yellow solid **TSA** (2.63 g, yield 81%). FT-IR (KBr, cm^{-1}): 3452 (s), 3357 (s), 2920 (s), 2212 (s), 1622 (s), 1515 (vs), 1492 (w), 1452 (w), 1301 (w), 1186 (s), 831 (s). ^{1}H NMR (400 MHz, $CDCl_3$) δ: 8.17 (d, J = 2.0 Hz, 1H), 8.01 (dd, J_1 = 8.8 Hz, J_2 = 2.4 Hz, 1H), 7.56(s, 1H), 7.50 (d, J = 8.8 Hz, 2H), 7.49 (s, 1H), 7.47 (d, J = 8.8 Hz, 2H), 7.18 (d, J = 8.4 Hz, 1H), 6.75 (d, J = 8.0 Hz, 2H), 6.73 (d, J = 8.4 Hz, 2H), 4.54 (s, H), 4.50 (s, 2H), 2.86 (s, 6H). ^{13}C NMR ($CDCl_3$, 100 MHz), δ: 154.28, 147.55, 147.27, 137.93, 136.61, 131.82, 129.31, 127.45, 127.18, 127.09, 127.00, 124.81, 118.78, 118.25, 117.86, 115.14, 111.45, 109.48, 44.43. LC-MS (APCI): m/z = 406.2014, calcd for $(C_{26}H_{24}N_5)^+$= 406.1953 ($[M+H]^+$).

3. Results and discussion

3.1 Synthesis and characterization of the samples

The synthetic routes of **TS**, **TSX** and **TSA** are illustrated in **Scheme 1**. **TS** was synthesized with Vilsmeier-Haack formylation reaction by using DMF and $POCl_3$. **TSX** was fabricated utilizing a typical Knoevenagel reaction of **TS** with 4-nitrophenylacetonitrile in the presence of piperidine as the catalyst. **TSA** was obtained *via* a reduction reaction by using compound **TSX** and $SnCl_2 \cdot 2H_2O$ in ethanol solution. **TSA** and its intermediates were characterized by FT-IR, ^{1}H NMR, ^{13}C NMR and mass spectroscopy, respectively. **TSA** could be dissolved easily in most organic solvents, such as benzene, DCM, tetrahydrofuran (THF), N,N-dimethylformamide (DMF) and dimethylsulfoxide (DMSO), but was insoluble in water.

3.2 The thermal property of TSA

To investigate the thermal stability of **TSA**, the thermogravimetric analysis (TGA) was carried out at a heating rate of 10 °C/min under nitrogen atmosphere. The result is shown in **Fig. S5**. As shown in **Fig. S5**, an obvious weight loss of **TSA** was located in the temperature range from 349 °C to 421 °C, the quickest decomposition temperature (T_{decomp}) occurred at 382 °C, the T_d value was 351 °C (T_d represents the temperature with 5% weight loss, and it is often used to estimate the thermal stability of a material[49-50]). The above data indicate that **TSA** is thermal stable below 340 °C and thus suitable for application of optical devices.

3.3 The photophysical properties of TSA

The optical properties of **TSA** in THF and solid state were tested, respectively. The UV-vis absorption and fluorescence spectra are displayed in **Fig. 1**. As showed in **Fig. 1**a, **TSA** in THF exhibited relatively broad band and the maximum absorption wavelength appeared at 387 nm. The extinction coefficient value (k) was higher with 10^4 $L \cdot cm^{-1} \cdot mol^{-1}$ (**Table 1**). The value suggested that the transform of electron of **TSA** was permitted. To gain an insight into the absorbing behavior of **TSA**, the theoretical characterization with density functional theory (DFT) was used. Geometry optimization of **TSA** was performed using the B3LYP/6-31G (d) basis set, while the electronic excitations corresponding to the absorption spectra were calculated using time-dependent-DFT (TD-DFT) by Gaussian 09.[51] The calculated value and experimental results of the absorption wavelength, oscillator strength, the main orbital contribution and energy gap are listed in **Table S1,** and the electron density distributions of the frontier molecular orbital are shown in **Fig. S**6. The theoretic absorption peak of **TSA** is located 401 nm, which is close to the experimental datum (387 nm) obtained from absorption spectra. By investigating the frontier molecular orbital (FMO) energy levels of **TSA**, the absorption band at 401 nm predicted that it had a sum of two main electronic transition modes H-1→L (56%) and H→L + 1 (26%), which could be ascribed to the combination of π-π* and intramolecular charge transfer (ICT) transition. In addition, by comparison with the absorption spectrum of **TSA** in THF, the broader absorption band with obvious bathochromic shift of **TSA** in the solid state was observed (**Fig. 1**a). This could be attributed to the increasing of π-conjugation length in its solid state due to the molecular stacking.[52] As showed in **Fig. 1**b, **TSA** has fluorescence emission both in solution and in solid state. The maximum emission peaks are located at 520 nm and 529 nm, respectively. In addition, the quantum efficiencies of TSA in THF solution and solid state were 4% and 28%, respectively.

Table 1 The linear optical physical parameters of **TSA** in different solvents

Sample	Solvents	$\lambda_{max}^{[a]}$	$\lambda_{max}^{[b]}$	K ($\times 10^4$)[c]	$\Delta\nu$ [d]
TSA in solution	benzene	380	514	4.09	6860
	DCM	378	527	4.15	7480
	THF	387	520	4.39	6609
	EA	382	524	4.27	7094
	ethanol	387	540	4.24	7321
	AN	375	536	3.91	8010
	DMF	394	540	4.11	6862
TSA in solid state		425	529	10.12	4554

[a] Peak position of the maximum absorption band. [b] Peak position of fluorescence emission, excited at the absorption maximum, [c] Molar absorptivity ($L \cdot cm^{-1} \cdot mol^{-1}$). [d] Stokes' shift in cm^{-1}.

View Article Online
DOI: 10.1039/C8TC02973C

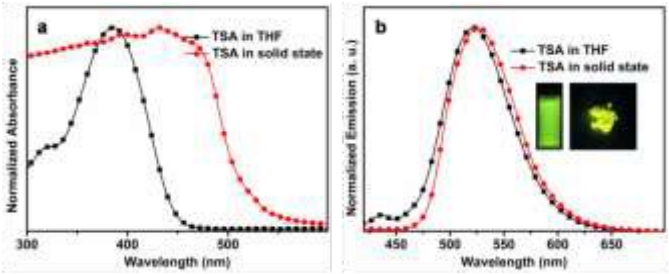

Fig. 1 The UV-vis (a) and PL (b) spectra of **TSA** (1.0×10^{-5} M) in THF solution and in solid state, Insert: photographs of fluorescence emission of **TSA** in solution and in solid state.

3.4 The solvent effect

The solvent polarity dependence of the fluorophores is more important in fluorescent field. Thus the solvatochromic behaviors of **TSA** were also studied in various solvents with increasing polarity. The results are displayed in **Fig. 2**. From **Fig. 2** (a), UV-vis absorption spectra showed slight bathochromic (from 380 nm to 394 nm) by increasing the solvent polarity. As can be seen in **Fig. 2** (b), with increasing of the solvent polarity, the emission bands exhibited an obvious bathochromic (from 514 nm to 540 nm). The fluorescent photos of **TSA** in different polar solvents (**Fig. 2** d) also demonstrated the same red-shifted fluorescence emissive phenomenon. The Lippert-Mataga plot (**Fig. 2** c) of Stokes' shift against the orientation polarizability of the solvent gave an upward straight line with a small slope (slope = 2227). The results indicate that the dipole moment of the **TSA** molecule in excited state is larger than that in ground state. The main reason is attributed to an ICT between the electron-donating and the accepting group in the molecular structure.

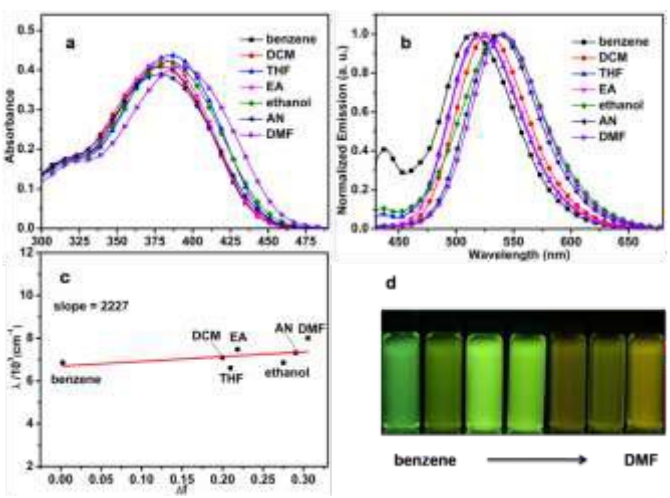

Fig. 2 (a) The UV-vis and (b) PL spectra, (c) Lippert-Mataga plotof **TSA** in solvents with different polarities. Concentration: 10 μM, excitation wavelength with the maximum absorption. (d) Insert: the photograph of fluorescent change of **TSA** in different solvents under irradiation at 365 nm. Abbreviations: Δν-Stokes' shifts, Δf -orientation, polarizability - $(\varepsilon - 1)/(2\varepsilon + 1)-(n^2 - 1)/(2n^2 + 1)$, where ε - dielectric constant and n - refractive index.

3.5 Multi-stimuli responsive fluorescence

3.5.1 Stimuli-responsive fluorescence for acid/base

In consideration of the basicity of the nitrogen atom in the structure of **TSA**, the molecule should be protonated and deprotonated in the presence of acid and base.[53-55] Therefore, the acid/base stimuli-responsive fluorescence was investigated not only in solutions such as benzene, DCM, trichloromethane, ethyl acetate (EA), ethanol, acetonitrile (ACN), DMF and DMSO but also in solid state. It is found that **TSA** possessed remarkable acidochromic behavior stimulating by TFA, hydrochloric acid and/or their vapors.

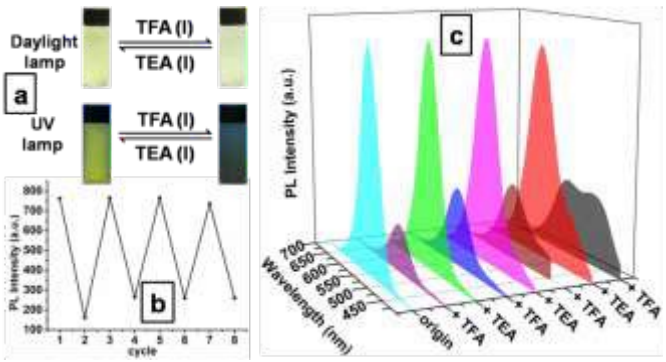

Fig. 3 (a) Photos of **TSA** in ACN were taken under daylight and UV lamp (365 nm). (b) Change in the emission intensity of **TSA** in ACN by repeated treated with TFA or TEA. (c) Change in the PL spectra of **TSA** between 'off' and 'on' by reversibly treated with TFA-TEA.

As showed in **Fig. 3**, as **TFA** was added to the solution of **TSA** in ACN, the obvious naked-eye color changing could be observed from yellow-green to light, moreover the emission spectra were slightly red-shifted accompanied by strong quenching of luminescence. Furthermore, with addition of excess TEA into the above solution, the fluorescence emission could be recovered to the original one. The fluorescence emission could be switched between 'on' and 'off' by alternately treating with TEA-TFA solvents without attenuation for many times. The results verify that **TSA** can be used as an indicator for acid/base in solution state.

View Article Online
DOI: 10.1039/C8TC02973C

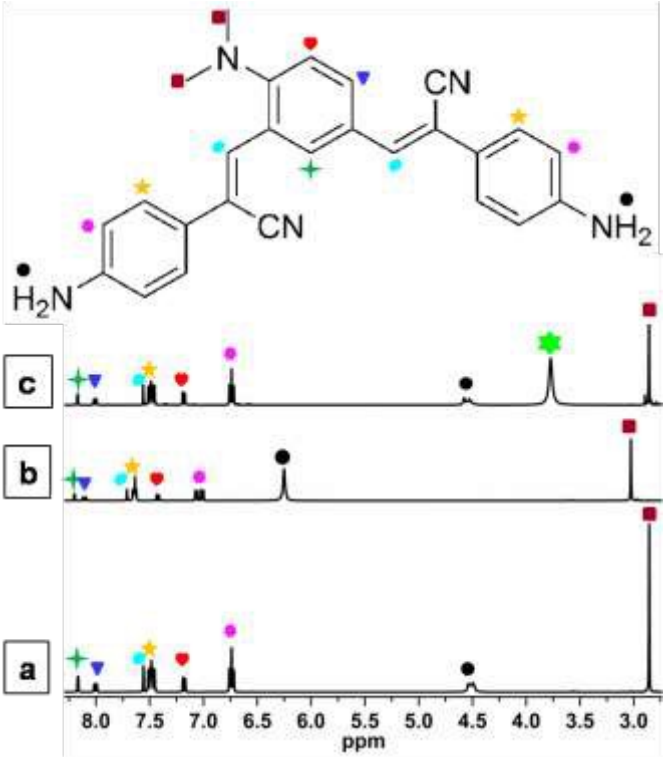

Fig. 4 The ^{1}H NMR spectra of (a) **TSA** (10 μM), (b) **TSA** (10 μM) + 4 equiv. TFA and (c) **TSA** (10 μM) + 4 equiv. TFA + excess TEA in CD_3CN. ✱ is the peak of H^+ of TEA.

To prove the reversible transformation of protonation and deprotonation, the ^{1}H NMR spectra were investigated (**Fig. 4**). When 4.0 equiv. of TFA was added to the **TSA** solution in $CDCl_3$, the protons of **TSA** shift downfield in the ^{1}H NMR spectra because of the transformation of **TSA** into an electron-deficient form **TSA**-H^+. After adding excess TEA into the above solution, the ^{1}H NMR spectrum was recovered fully to the original one, suggesting that the transformation between **TSA** and **TSA**-H^+ was completely reversible and essentially non-destructive in nature.

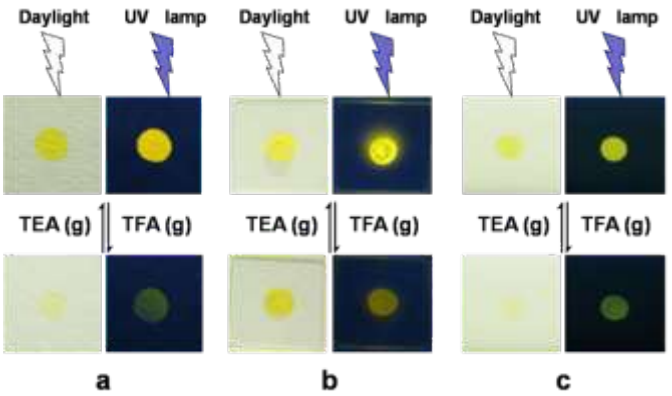

Fig. 5 Recycling of the fluorescence emission and color switching of **TSA** in solid state upon fuming with TFA (bottom) and TEA (up) vapors. **TSA** spots on the filter paper (a), the quartz glass slide (b) and the TLC plate(c). The photos were taken under daylight (left) and UV lamp (right, 365 nm) respectively.

Additionally, the stimuli-responsive fluorescence of **TSA** in solid state for acid/base was also investigated. The results are shown in **Fig. 5**. In these experiments, the sample was deposited on the filter paper (a), the quartz glass slide (b) and the TLC plate (c) by **TSA** in DCM, respectively. After being dried and fumed with TFA vapor in turn, the dye spots were immediately turned from brilliant yellow to orange (b) or/and obscure (a, c), and the fluorescence intensity changed to weak. The above phenomenon could be quickly converted back to their original forms as they were treated with TEA vapor. This reversible change could repeat many times in spite of slight attenuation of the fluorescent intensity *via* alternately fuming with TFA and TEA vapors. The results indicate that **TSA** has the potential in application as a solid-state fluorescence switching material.

3.5.2 Mechanical grinding responsive fluorescence

It is well known that MFC behavior can be achieved by the transformation of the molecular conformation, packing mode, etc.[56-61] Thus, the feature of stimuli-responsive luminescence switching was performed by grinding in a mortar with a pestle. As showed in **Fig. 6**, the as-synthesized **TSA** was a yellow crystalline powder with bright fluorescence (λ_{em} = 529 nm). After grinding, an orange powder with weak orange-yellow fluorescence (λ_{em} = 549 nm) was detected. The grinding treatment could cause a spectral red-shift of ca. 20 nm before and after grinding. Interestingly, when DCM was dropped in mortar, the color and fluorescence emission of the ground powder were recovered immediately (the inset photos in **Fig. 6**). To investigate the reversibility of the MFC effect, the drying powder was ground again after DCM being evaporated at room temperature. The ground sample changed back to orange powder. This reversible cycle of fluorescence switching by mechanical grinding could repeat many times, suggesting the good stability of **TSA**.

To further obtain the fluorescence excited-state decay information of **TSA** in solid state before and after grinding, the time-resolved emission-decay behaviors were measured. The fluorescence decay curves and the lifetime data are illustrated in **Fig. S7**. For initial sample, the fluorescence lifetime is estimated to be 0.6 ns, while the value is 1.22 ns of its ground sample. We speculated that the difference of molecular conformation and arrangements in their aggregation state resulted in the change of fluorescence lifetime. The result indicates that the fluorescence lifetime of **TSA** solid can also be adjusted by grinding.

View Article Online
DOI: 10.1039/C8TC02973C

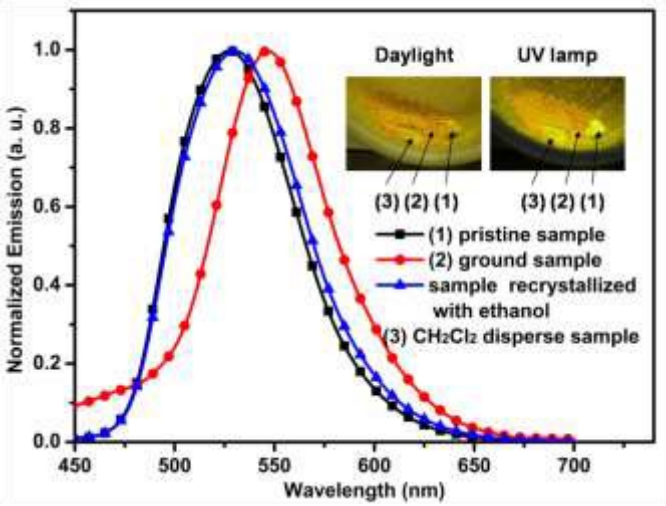

Fig. 6 The normalized emission spectra of the corresponding samples, inset: photographic images of the corresponding samples under irradiation of daylight and UV light lamp: (1) pristine sample, (2) ground sample, (3) ground sample upon addition of DCM.

To study the mechanism of the MFC phenomenon of **TSA**, the PXRD and DSC tests were carried out. The results are shown in **Fig. 7**a. From **Fig. 7**a, the diffraction pattern of the initial powder showed sharp and intense reflections, indicating that the aggregate was ordered well in the crystalline powders. After grinding, the original sharp and intense diffraction peaks attenuated or even disappeared, which revealed that the initial orderly arrangement was destroyed. After recrystallization in ethanol, the diffraction patterns of the powders were essentially same with that of pristine powder. The result reveals that the microcrystalline structure of powders has been recovered basically. The above PXRD results confirm that the reversible transition between the ordered and disordered molecular aggregation is crucial for the MFC behaviors.

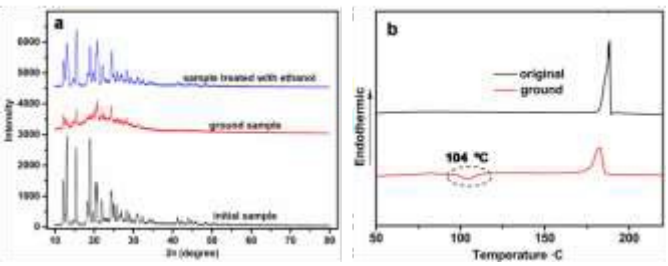

Fig. 7 (a) PXRD patterns of initial, ground and recrystallized with ethanol sample of **TSA**. (b) DSC curves of **TSA** before and after grind.

As can be seen in **Fig. 7**b, the differential scanning calorimetry (DSC) curve for the heating pristine sample of **TSA** had a clear melting endothermic peak at 188 °C and no exothermic peak was found, which manifested the crystalline morphology of **TSA**. In contrast, the ground state of **TSA** revealed an additional exothermic recrystallization peak at 104 °C, which predicted that the **TSA** crystal was partially destroyed and converted to an amorphous state and ground sample was partially in a metastable amorphous state by the grinding. The DSC result demonstrates that grinding can convert thermodynamically stable crystals into metastable state.[62-63]

Fig. 8 SEM images of polymorphs**TSA** (Magnification = 1800). (a) presents the initial sample, (b) presents ground sample and (c) presents sample recrystallized with ethanol.

The morphological changes of polymorphs **TSA** from the crystalline state to the amorphous state were collected by SEM, and the results are shown in **Fig. 8**. As showed in **Fig. 8**, the initial sample presented rod-like morphology, but the ground sample presented amorphous state. However, after recrystallization of the ground sample with ethanol, it recovered essentially into the original pattern of the rod-like morphology. All the above results authenticate that **TSA** is a very promising MFC material.

4. Application of TSA

4.1 Fluorescence sensor for acid/base and PA

The investigation of stimuli-responsive fluorescence for acid/base (in **3.5.1** section) indicates that **TSA** can be used as fluorescence sensor for acid/base. It prompts us to explore the potential application of **TSA** as a sensory material for the detection of PA.

Based on the fluorescence quenching effect for acidic materials, the recognition behavior of **TSA** towards the selected acidic explosive aromatic nitro compounds (NACs) was investigated in ethanol/water mixture (f_w = 5%). As shown in **Fig. S8**, approximately 60% quenching of the fluorescence intensity occurred when 4 equivalents of PA were titrated. However, other NACs did not exceed 20% when keeping the same equivalents, it indicated that **TSA** exhibited selectivity toward PA. The main reason for this is that PA exhibits acidity in an aqueous system, and can combine with the amino group. And other NACs only exhibit weak acidity or neutral behavior, and cannot bond with **TSA**. The results suggested that compound **TSA** can be used as a chemosensor for PA.

To investigate the property of the **TSA** recognizing PA, the titration experiments were carried out in ethanol/water mixture

View Article Online
DOI: 10.1039/C8TC02973C

(f_w = 5%) by adding aliquots of PA. As showed in **Fig. 9**, by adding PA amount from 0 to 4 equiv. to the solution of **TSA** (10 μM), it was observed the increasing of the absorption intensity with slight blue-shift and the quenching of the fluorescence emission. The detection limit (DL) for PA was about 300 ppb calculating according to the DL = 3δ/S (δ is the standard deviation of the blank solution and S is the slope of the calibration plot). The results indicate that **TSA** can act as the fluorescence sensor for PA, even in the ppb concentration level. This can be rationalized as follows. As a strong acid, the PA has an obvious tendency to transfer proton of hydroxyl groups to the basic of amino or N,N-dimethylamino group which makes an electrostatic complex between **TSA** and PA. This strong complexation between the **TSA** and PA facilitates the photoinduced electron transferring, so as to shift the electron to a nonradiating decay path and quench fluorescence emission.

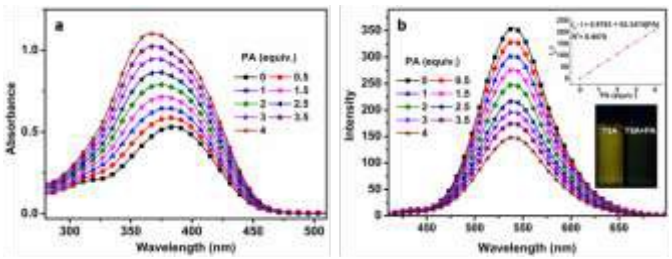

Fig. 9 The changes of absorption (a) and fluorescence (b) spectra of compound **TSA** (10 μM) with increasing the concentrations of PA in ethanol/water mixture (f_w = 5%), Inset: linear equation plots of I_0-I versus [PA] in ethanol/water mixture (f_w = 5 %); I_0 is the peak intensity of **TSA**, and I is the peak intensity of **TSA** after addition of PA (0-4 equiv.).

4.2 Rewritable data storage

Information processing including recording, storage and security technologies of data has become an integral part of the human life. Based on the above reversible mechanical-responsive luminescence switching features (in **3.5.3** section), the technology of rewritable information storage was designed. The results are displayed in **Fig. 10**. In **Fig. 10**, the mechanical friction, the solvent and vapor of DCM were utilized to realize the rewritable data storage. **TSA** was coated on typing paper using the suspension of DCM and dried at room temperature. The letters 'An Da' with orange light and weak fluorescence resulting from the amorphous structure were written on the **TSA** with a glass rod. Then the letters were easily erased by grinding on the bright background. In the next picture, the "Huai Shi" with yellow (under daylight) and strong kelly fluorescence (under UV lamp) revealed clearly by using a cotton swab and DCM solvent as pen and ink, respectively. Following the weak emission background can quickly be erased after using fuming treatment with DCM vapor. By repeating the steps above, the reversible writing and erasing of different fluorescent letters were performed. The results indicate that **TSA** is a very promising candidate for application in data storage.

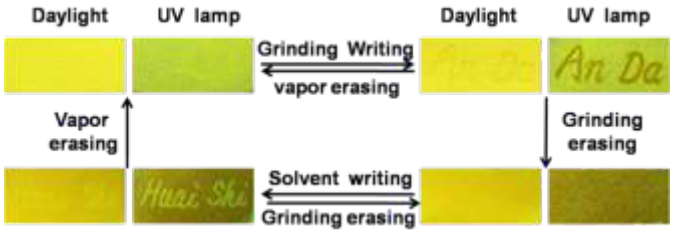

Fig. 10 Photographs of the writing/erasing cycle under daylight and UV light lamp.

4.3 White light-emitting diode (w-LED)

Owing to the preferable fluorescence emission in solid state of **TSA**, the w-LED was fabricated. The detailed LED packaging process contains the following main steps: Firstly, the as-synthesized **TSA** (20 mg) was mixed thoroughly with silicone encapsulant (5 g, 1:1 weight ratios of silicone A to silicone B) in a small beaker. Then, the obtained **TSA**–silicone mixture was degassed using vacuum, and then coated on the surface of a commercial InGaN blue-emitting chip. Finally, the encapsulation was solidified at 150 ºC for 1 h. The chromaticity feature and optical performance of the prototype device were measured. The results are displayed in **Fig. 11**. From **Fig. 11**, the w-LED exhibited a correlated color temperature (CCT, 7544 K), a color rendering index (CRI, Ra = 70.2) and a luminous efficacy (LE, 25.41 lm/W) under a 150 mA current. The calculated chromaticity coordinate (x, y) in CIE 1931 chromaticity space was (0.2912, 0.3418), which is in the cold white region. The results demonstrate that the **TSA** has the potential ability to apply to w-LED.

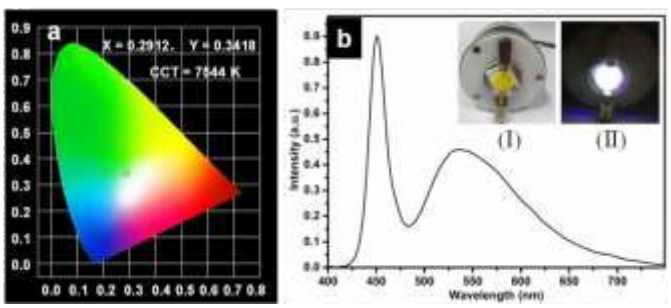

Fig. 11 (a) CIE chromaticity diagram of the fabricated w-LED. (b) Electroluminescent spectra of the fabricated w-LED, insets show the photographs of the fabricated w-LED driven without (I) and with (II) a 150 mA current.

5. Conclusions

A novel Λ-shaped α-cyanostilbene derivative (**TSA**) was designed and synthesized successfully. The photophysical and multi-stimuli-responsive properties of **TSA** were investigated

View Article Online
DOI: 10.1039/C8TC02973C

thoroughly. The results indicate **TSA** has fluorescence emission both in solution and solid state. The color and fluorescence emission of **TSA** could be switched by external stimuli including acid/base, PA and grinding. **TSA** could be used to recognize PA in the mixture of EtOH-H_2O, with a detection limit of 300 ppb, and it could also be utilized as fluorescence sensor for acid/base and as information data storage material. Moreover, the **TSA** had desirable potential application in w-LED by sealing **TSA** on blue chips.

Acknowledgements

This work was supported by the National Natural Science Foundation of China (51673001, 51432001) and the Educational Commission of Anhui Province of China (KJ2014ZD02).

Notes and references

[a]*College of Chemistry & Chemical Engineering, Key Laboratory of Functional Inorganic Materials of Anhui Province, Anhui University, Hefei 230601, PR China. *E-mail: jxyang@ahu.edu.cn.*

[b]*School of Chemical and Materials Engineering of Huainan Normal University, Anhui, Huainan 232038, PR China.*

[c]*State Key Laboratory of Crystal Materials, Shandong University, Jinan 502100, PR China*

1 P. Alam, V. Kachwal and I. R. Laskar, *Sens. Actuators B*, 2016, **228**, 539-550.
2 J. L. Shen, J. Y. Pang, G. Y. Xu, X. Xin, Y. J. Yang, X. Y. Luan and S. L. Yuan, *RSC Adv.*, 2016, **6**, 11683-11690.
3 V. M. Vijayan, S. J. Shenoy, S. P. Victor and J. Muthu, *Colloids and Surfaces B: Biointerfaces*, 2016, **146**, 84-96.
4 Q. Wan, K. Wang, C. B. He, M. Y. Liu, G. J. Zeng, H. Y. Huang, F. J. Deng, X. Y. Zhang and Y. Wei, *Polym. Chem.*, 2015, **6**, 8214-8221.
5 Q. X. Hua, B. Xin, J. X. Liu, L. X. Zhao, Z. J. Xiong, T. Chen, Z. Q. Chen, C. Li, W. L. Gong, Z. L. Huang and M. Q. Zhu, *Faraday Discuss.*, 2017, **196**, 439-454.
6 J. R. Kumpfer and S. J. Rowan, *J. Am. Chem. Soc.*, 2011, **133**, 12866-12874.
7 P. Ceroni, A. Credi and M. Venturi, *Chem. Soc. Rev.*, 2014, **43**, 4068-4083.
8 X. F. Mei, G. X. Wen, J. W. Wang, H. M. Yao, Y. Zhao, Z. H. Lin and Q. D. Ling, *J. Mater. Chem. C*, 2015, **3**, 7267-7271.
9 Y. B. Zhou, Y. Z. Liu, Y. Guo, M. C. Liu, J. X. Chen, X. B. Huang, W. X. Gao, J. C. Ding, Y. X. Cheng and H. Y. Wu, *Dyes Pigments*, 2017, **141**, 428-440.
10 Y. F. Huo, L. N. Zhu, X. Y. Li, G. M. Han and D. M. Kong, *Sens. Actuators B*, 2016, **237**, 179-189.
11 Y. Wu, Y. S. Xie, Q. Zhang, H. Tian, W. H. Zhu and A. D. Q. Li, *Angew. Chem. Int. Ed.*, 2014, **53**, 2090-2094.
12 Z. G. Chi, X. Q. Zhang, B. J. Xu, X. Zhou, C. P. Ma, Y. Zhang, S. W. Liu and J. R. Xu, *Soc. Rev.*, 2012, **41**, 3878-3896.
13 P. S. Hariharan, V. K. Prasad, S. Nandi, A. Anoop, D. Moon and S. P. Anthony, *Cryst. Growth Des*., 2017, **17**, 146-155.
14 S. J. Lim, B. K. An, S. D. Jung, M. A. Chung and S. Y. Park, *Angew. Chem. Int. Ed*., 2004, **43**, 6346-6350.
15 W. Y. Fang, Y. Y. Zhang, G. B. Zhang, L. Kong, L. M. Yang and J. X. Yang, *CrystEngComm*, 2017, **19**, 1294-1303.
16 R. Zheng, X. F. Mei, Z. H. Lin, Y. Zhao, H. M. Yao, W. Lv and Q. D. Ling, *J. Mater. Chem. C*, 2015, **3**, 10242-10248.
17 T. Y. Han, X. Feng, D. D. Chen and Y. P. Dong, *J. Mater. Chem. C*, 2015, **3**, 7446-7454.
18 S. A. Sharber, K. C. Shih, A. Mann, F. Frausto, T. E. Haas, M. P. Nieh and S. W. Thomas, *Chem. Sci.*, DOI: 10.1039/c8sc00980e.
19 Y. Ma, S. J. Liu, H. R. Yang, Y. Zeng, P. F. She, N. Y. Zhu, C. L. Ho, Q. Zhao, W. Huang and W. Y. Wong, *Inorg. Chem*,. 2017, **56**, 2409−2416.
20 W. P. Lin, Q. Zhao, H. B. Sun, K. Y. Zhang, H. R. Yang, Q. Yu, X. H. Zhou, S. Guo, S. J. Liu and W. Huang, *Adv. Opt. Mater.*, 2015, **3**, 368-375.
21 Q. Zhao, W. J. Xu, H. B. Sun, J. G. Yang, K. Y. Zhang, S. J. Liu, Y. Ma and W. Huang, *Adv. Opt. Mater.*, 2016, **4**, 1167-1173.
22 X. L. Lu and M. Xia, *J. Mater. Chem. C*, 2016, **4**, 9350-9358.
23 W. Z. Yuan, Y. Q. Tan, Y. Y. Gong, P. Lu, J. W. Y. Lam, X. Y. Shen, C. F. Feng, H. H. Sung, Y. W. Lu, I. D. Williams, J. Z. Sun, Y. M. Zhang and B. Z. Tang, *Adv. Mater.* 2013, **25**, 2837-2843.
24 J. Zhao, Z. H. Chi, Y. Zhang, Z. Mao, Z. Y. Yang, E. Ubba and Z. G. Chi, *J. Mater. Chem. C*, DOI: 10.1039/c8tc01648h.
25 Y. Ma, P. F. She, K. Y. Zhang, H. R. Yang, Y. Y. Qin, Z. H. Xu, S. J. Liu, Q. Zhao and W. Huang, *Nat. Commun.*, 2018, **9**, 3.
26 H. B. Sun, S. J. Liu, W. P. Lin, K. Y. Zhang, W. Lv, X. Huang, F. W. Huo, H. R. Yang, G. Jenkins, Q. Zhao and W. Huang, *Nat. Commun*., 2014, **3**, 3601
27 K. Y. Zhang, X. J. Chen, G. L. Sun, T. W. Zhang, S. J. Liu, Q. Zhao and W. Huang, *Adv. Mater*., 2016, **28**, 7137-7142.
28 M. Martinez-Abadia, R. Gimenez and M. B. Ros, *Adv. Mater.*, 2018, **30**, 1704161.
29 Y. W. Ma, Y. Li, L. G. Chen, Y. Xiong and G. H. Yin, *Dyes Pigm*., 2016, **126**, 194-201.
30 W. Y. Fang, G. B. Zhang, J. Chen, L. Kong, L. M. Yang, H. Bi and J. X. Yang, *Sens. Actuators B*, 2016, **229**, 338-346.
31 L. Zhou, D. F. Xu, H. Z. Gao, A. X. Han, Y. Yang, C. Zhang, X. L. Liu and F. Zhao, *RSC Adv.*, 2016, **6**, 69560-69568.
32 X. Y. Shen, Y. J. Wang, E. G. Zhao, W. Z. Yuan, Y. Liu, P. Lu, A. J. Qin, Y. G. Ma, J. Z. Sun and B. Z. Tang, *J. Phys. Chem. C*, 2013, **117**, 7334-7347.
33 H. Z. Gao, D. F. Xu, X. L. Liu, A. X. Han, L. Zhou, C. Zhang, Y. Yang and W. L. Li, *RSC Adv.*, 2017, **7**, 1348-1356.
34 Z. G. Xia and Q. L. Liu, *Prog. Mater. Sci*,. 2016, **84**, 59-117.
35 K. Li, M. M. Shang, H. Z. Lian and J. Lin, *J. Mater. Chem. C*, 2016, **4**, 5507-5530.
36 C. C. Lin, A. Meijerink and R. S. Liu, J. Phys. *Chem. Lett.*, 2016, **7**, 495-503.
37 X. Y. Huang, *Nat. Photonics*, 2014, **8**, 748-749.
38 P. Pust, P. J. Schmidt and W. Schnick, *Nat. Mater.*, 2015, **14**, 454-458.
39 H. M. Zhu, C. C. Lin, W. Q. Luo, S. T. Shu, Z. G. Liu, Y. S. Liu, J. T. Kong, E. Ma, Y. G. Cao, R. S. Liu and X. Y. Chen, *Nat Commun*., 2014, 4312.

View Article Online
DOI: 10.1039/C8TC02973C

40 B. Wang, H. Lin, J. Xu, H. Chen and Y. S. Wang, *ACS Appl. Mater. Interfaces*, 2014, **6**, 22905-22913.

41 J. S. Zhong, H. B. Gao, Y. J. Yuan, L. F. Chen, D. Q. Chen and Z. G. Ji, *Jalloys Compd.*, 2018, **735**, 2303-2310.

42 X. Ding, G. Zhu, W. Y. Geng, Q. Wang and Y. H. Wang, *Inorg. Chem.*, 2016, **55**, 154-162.

43 B. Wang, H. Lin, F. Huang, J. Xu, H. Chen, Z. B. Lin and Y. S. Wang, *Chem. Mater.*, 2016, **28**, 3515-3524.

44 P. F. Smet, A. B. Parmentier and D. Poelman, *J. Electrochem. Soc.*, 2011, **158**, R37-R54.

45 J. Meyer and F. Tappe, *Adv. Optical Mater.*, 2015, **3**, 424-430.

46 J. Chen, Y. G. Liu, L. F. Mei, H. K. Liu, M. H. Fang and Z. H. Huang, *SCI REP-UK.*, 2015, 1-9.

47 C. W. Liao, R. Rao M. and S. S. Sun, *Chem. Commun.*, 2015, **51**, 2656-2659.

48 X. L. Zhu, R. Liu, Y. H. Li, H. Huang, Q. Wang, D. F. Wang, X. Zhu, S. S. Liu and H. J. Zhu, *Chem. Commun.*, 2014, **50**, 12951-12954.

49 L. Kong , J. X. Yang, H. P. Zhou , S. L. Li, F. Y. Hao, Q. Zhang, Y. L. Tu, J. Y. Wu, Z. M. Xue and Y. P. Tian, *Sci China Chem*, 2013, **56**, 106-116.

50 H. Y. Li, Z. G. Chi, X. Q. Zhang, B. J. Xu, S. W. Liu, Y. Zhang and J. R. Xu, *Chem. Commun.*, 2011, **47**, 11273-11275.

51 M. J. Frisch, G. W. Trucks, H. B. Schlegel, G. E. Scuseria, M. A. Robb, J. R. Cheeseman, G. Scalmani, V. Barone, B. Mennucci, G. A. Petersson, H. Nakatsuji, M. Caricato, X. Li, H. P. Hratchian, A. F. Izmaylov, J. Bloino, G. Zheng, J. L. Sonnenberg, M. Hada, M. Ehara, K. Toyota, R. Fukuda, J. Hasegawa, M. Ishida, T. Nakajima, Y. Honda, O. Kitao, H. Nakai, T. Vreven, J. A. Montgomery Jr., J. E. Peralta, F. Ogliaro, M. Bearpark, J. J. Heyd, E. Brothers, K. N. Kudin, V. N. Staroverov, R. Kobayashi, J. Normand, K. Raghavachari, A. Rendell, J. C. Burant, S. S. Iyengar, J. Tomasi, M. Cossi, N. Rega, J. M. Millam, M. Klene, J. E. Knox, J.B. Cross, V. Bakken, C. Adamo, J. Jaramillo, R. Gomperts, R. E. Stratmann, O. Yazyev, A. J. Austin, R. Cammi, C. Pomelli, J. W. Ochterski, R. L. Martin, K. Morokuma, V. G. Zakrzewski, G. A. Voth, P. Salvador, J. J. Dannenberg, S. Dapprich, A. D. Daniels, O. Farkas, J. B. Foresman, J. V. Ortiz, J. Cioslowski, D. J. Fox, Gaussian 09, Revision A.1, Gaussian Inc., Wallingford CT, 2009.

52 X. L. Zhu, H. Huang, R. Liu, X. D. Jin, Y. H. Li, D. F. Wang, Q. Wang and H. J. Zhu, *J. Mater. Chem. C*, 2015, **3**, 3774-3782.

53 H. Sakai, T. Kubota, J. Yuasa, Y. Araki, T. Sakanoue, T. Takenobu, T. Wada, T. Kawai and T. Hasobe, *Org. Biomol. Chem.*, 2016, **14**, 6738-6743.

54 Z. M. Wang, H. Nie, Z. Q. Yu, A. J. Qin, Z. J. Zhao and B. Z. Tang, *J. Mater. Chem. C*, 2015, **3**, 9103-9111.

55 S. Wang, S. Z. Xiao, X. H. Chen, R. H. Zhang, Q. Cao and K. Zou, *Dyes Pigments*, 2013, **99**, 543-547.

56 X. Q. Zhang, Z. Y. Ma, Y. Yang, X. Y. Zhang, X. R. Jia and Y. Wei, *J. Mater. Chem. C*, 2014, **2**, 8932-8938.

57 K. Wang, H. Y. Zhang, S. Y. Chen, G. C. Yang, J. B. Zhang, W. J. Tian, Z. M. Su and Y. Wang, *Adv. Mater.*, 2014, **26**, 6168-6173.

58 C. Wang, B. Xu, M. Li, Z. Chi, Y. Xie, Q. Li and Z. Li, *Mater. Horiz.*, 2016, **3**, 220-225.

59 S. Varughese, *J. Mater. Chem. C*, 2014, **2**, 3499-3516.

60 C. Botta, S. Benedini and L. Carlucci, *J. Mater. Chem. C*, 2016, **4**, 2979-2989.

61 Y. X. Lei, Y. Z. Liu, Y. Guo, J. X. Chen, X. B. Huang, W. X. Gao, L. B. Qian, H. Y. Wu, M. C. Liu and Y. X. Cheng, *J. Phys. Chem. C*, 2015, **119**, 23138-23148.

62 B. J. Xu, J. J. He, Y. X. Mu, Q. Z. Zhu, S. K. Wu, Y. F. Wang, Y. Zhang, C. J. Jin, C. C. Lo, Z. G. Chi, A. Lien, S. W. Liu and J. R. Xu, *Chem. Sci.*, 2015, **6**, 3236-3241.

63 P. Galer, R. C. Korošec, M. Vidmar and B. Šket, *J. Am. Chem. Soc.*, 2014, **136**, 7383-7394.

View Article Online
DOI: 10.1039/C8TC02973C